Title
Resonant Pneumatic Tactile Sensing for Soft Grippers

Journal
IEEE Robotics and Automation Letters, 7(4)

ISSN
2377-3766

Authors
Li, Monica S
Huh, Tae Myung
Yahnker, Christopher R
et al.

Publication Date
2022

DOI
10.1109/lra.2022.3191186

Resonant pneumatic tactile sensing for soft grippers

Monica S. Li[1*], Tae Myung Huh[1], Christopher R. Yahnker[2], and Hannah S. Stuart[1]

***Abstract*—Soft robots capable of dexterous manipulation can enable the exploration of extreme environments. Equipping these robots with tactile sensing is a challenge, as sensors must be flexible, stretchable, and robust to environmental conditions. We present a tactile sensor design with a pneumatically driven acoustic resonator, without electronics near from the end-effector. For applications to soft grippers, we measure the resonant frequency of a soft tube undergoing stretching and bending. A small hole along the resonant tube enables contact sensing and pretouch up to 2 mm away. We also measure resonant frequency for a rigid uni-axial force sensing probe. Grasping tasks utilize three sensing modalities of a soft gripper; finger pose, fingertip contact, and force in the palm all provide feedback for dexterous manipulation. We discuss and address in future work the effects of atmosphere and air flow rate on resonant frequency as well as limitations in signal processing of this sensor design.**

***Index Terms*—Soft Sensors and Actuators, Grasping, Force and Tactile Sensing, Robotics in Hazardous Fields**

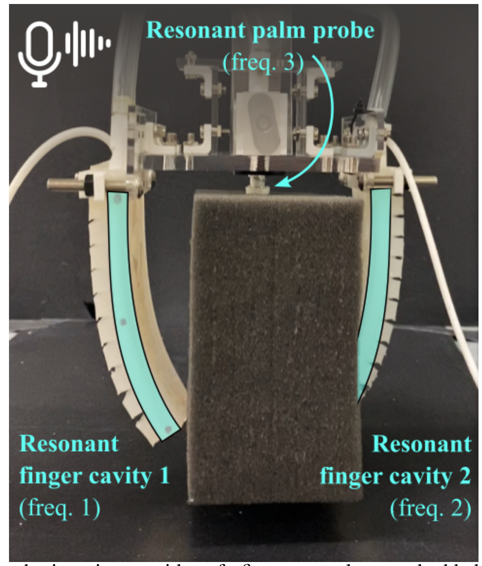

Fig. 1: A robotic gripper with soft fingers employs embedded pneumatic resonance-based acoustic tactile sensors. Each finger can detect pose and contact, while a probe in the palm measures force. The single remotely located microphone simultaneously monitors the emitted resonant frequency of each sensor. The gripper has no integrated electronic components.

I. Introduction

Soft robotic hands and grippers enable gently adaptive interactions through underactuation and compliant and deformable materials. These designs are already demonstrated in a wide range of potential applications – for example, soft hands can be particularly well suited to field missions when the end-effector must be capable, gentle and physically resilient [1], [2]. Equipping soft robots with a "sense of touch" is an active development area that enables new adaptive control methods for manipulation tasks [3].

While soft pneumatic robots have demonstrated survivability and operation in extreme conditions like snow, fire, and large external loads [4], challenges remain regarding the integration of electronics and sensors into articulated soft structures, discussed in [5]. New fabrication methods continue to emerge in order to integrate electronic sensors with soft actuators. Recent soft sensing works include additive manufacturing with conductive filaments [6] and with embedded electronic sensors [7], and screen printing with piezoresistive materials [8], [9]. Other sensing modalities include a camera on the end of a growing vine robot for steering and locomotion [10]. A microphone embedded in a soft finger detects where and what the finger is tapping [11]. A challenge is to reduce the effects that large, repetitive strains, and resulting fatigue, have on the function of sensitive electronics over extended use.

Additionally, electronics may be unsuitable for some conditions, such as in easily combustible atmospheres (gas tanks, mine shafts) or in sensitive magnetic fields (MRI). An example of a recent trend towards soft robots that operate without electronics altogether includes pneumatic computation for gait control during locomotion [12], [13].

We present a new flexible tactile sensing modality, without electronics near the end-effector. Inspired by woodwind instruments, we integrate resonant tubes in the soft fingers and palm of a gripper. Emitted acoustic frequencies, dependent on the geometry of these resonant tubes, provide information about pose and contact of the fingers and force at the palm, and are monitored by a remotely located microphone (Fig. 1). We note that people perceive acoustic emissions during dexterous manipulation, with studies showing that sound plays a role during haptic exploratory procedures [14]. In application, we envision a robot topology akin to the human ear, where the sounds emitted at a distal end-effector are perceived with a microphone on the body of a robot, proximal to the manipulator. To the authors' knowledge, this is the first presentation of

Manuscript received: February, 24, 2022; Revised June, 28, 2022; Accepted June, 13, 2022.

This paper was recommended for publication by Editor Yong-Lae Park upon evaluation of the Associate Editor and Reviewers' comments. M. Li is supported by the National Aeronautics and Space Administration grant No.80NSSC20K1166 through a Space Technology Research Fellowship. T. Huh is supported by the National Aeronautics and Space Administration under grant No.80NSSC21K0069, issued through the Early Career Faculty Program. Any opinions, findings, and conclusions or recommendations expressed in this material are those of the authors and do not necessarily reflect the views of the funding agencies.

[1]M.Li, T. M. Huh, and H. S. Stuart are with the Embodied Dexterity Group, Dept. of Mechanical Engineering, University of California at Berkeley, Berkeley, CA, USA monicasli@berkeley.edu

[2]C. R. Yahnker is with the Autonomous Systems (D34) Division, NASA Jet Propulsion Laboratory, California Institute of Technology, Pasadena, CA, USA

Digital Object Identifier (DOI): see top of this page.

tactile sensing where the signal travels through the atmosphere, and the end-effector has no electronics nor requires vision.

A. Overview

Section II provides the relevant theoretical background on acoustic resonance, with the measurand of frequency modulating as a function of cavity geometry. Section III describes the resonant tube geometries, acoustic measurements and processing methods employed throughout the experiments. We then present the implementation and calibration of specific resonant sensors analogous to the sub-components of a robotic gripper: (1) proprioceptive and contact sensors integrated into a soft finger in Section IV and (2) a force probe for the palm in Section V. In Section VI, we demonstrate the integrated gripper, as in Fig. 1, showing how multiple sensor readings can be detected simultaneously with a single off-board microphone. Future directions for this tactile technology are discussed in Section VII. Emphasized in Section VIII, such acoustic sensing holds great potential for soft, electronics-free end-effectors.

II. Acoustic theory

Instabilities of airflow across objects can generate pressure waves that emanate through the atmosphere. Under certain conditions, these pressure waves amplify in a feedback mechanism known as resonance [15]. We purposefully design a pneumatic resonator (Fig. 2). A constant pressure drop drives airflow through a narrow inlet, across an edge and into a tube. Airflow oscillates above and below the end, emanating as pressure waves into the ambient atmosphere. The frequency of oscillation is dependent on the geometry of the resonant tube. We focus on tube length for this sensor design, where stretch and compression change tube length and resonant frequency. Adding a small hole along the side of the tube affects resonant frequency as well. Resonant frequency is a function of additional parameters such as edge-orifice shape (*fipple*), atmosphere and flow rate, which are kept constant throughout this study.

A. Resonance of a closed tube with varying length

The resonant frequency can be approximated from the geometry of the tube. In the 1D wave propagation model of a closed-closed tube, the fundamental wavelength or first harmonic is twice the tube length. Higher harmonics are multiples of this fundamental harmonic. Resonant frequency f_r for a closed tube is

$$f_r = \frac{nc}{2L} \tag{1}$$

for harmonic integer $n = 1, 2, 3...$, speed of sound c, tube length L. Many geometric parameters of the resonant structure alter the emitted frequency, e.g., fipple shape. We focus on tube length as an analog to finger pose and force sensing.

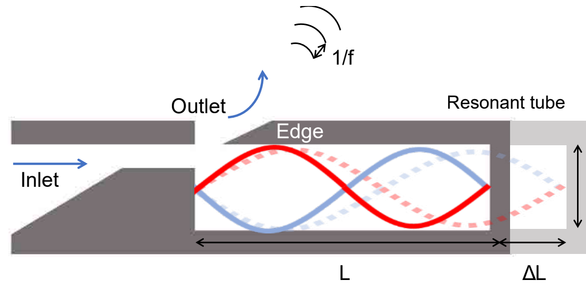

Fig. 2: Cross-sectional schematic of pneumatic resonant structure. Air flows in from the left and is constricted through a slit. Air flows out above the edge and into the tube, traveling the length of the tube and back. These oscillations create pressure waves, with the oscillating frequency f governed by the cavity length L. The waveform (blue/red curve) represents the second resonant mode (closed-closed) of the given cavity. Increasing the resonant cavity length ΔL decreases the emitted frequency.

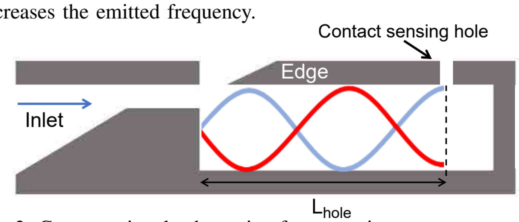

Fig. 3: Cross-sectional schematic of pneumatic resonant structure for contact sensing. An unobstructed contact sensing hole changes its local boundary condition to an antinode. Contact at the sensing hole reverts the resonance back to closed-closed regime of a non-perforated tube.

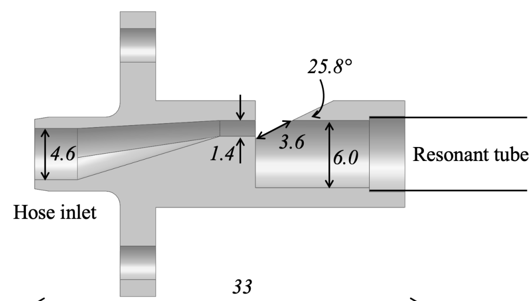

Fig. 4: Cross sectional image of fipple geometry, with distance units in (mm). Air flow enters through hose inlet from the left.

B. Resonance with small lateral opening

In addition to physically changing the resonant tube length, a lateral opening along the tube effectively changes the boundary condition, and thus the resonant modes and frequency. With a lateral hole as shown in Fig. 3, the hole location is likely in an antinode condition. Then the resonant mode n may be different from the mode without the hole, depending on the hole location. Computing actual f_r would require computational fluid dynamics solvers, which is beyond the scope of this paper.

We propose to detect contact of an object over the hole by measuring the difference of f_rs before and after the contact. It is also difficult to model the resonant mode of partially closed or air-leaking hole; we present an experimental result from gradual hole closing in Section IV-C.

III. Experimental methods & acoustic processing

Throughout this study we utilize a flow divider geometry upstream of the resonant tube. This fipple has a maximum stream-wise gap length of 3.6 mm and the edge angle is 28.5°, as in Fig. 4 and helps create the oscillating pressure waves we

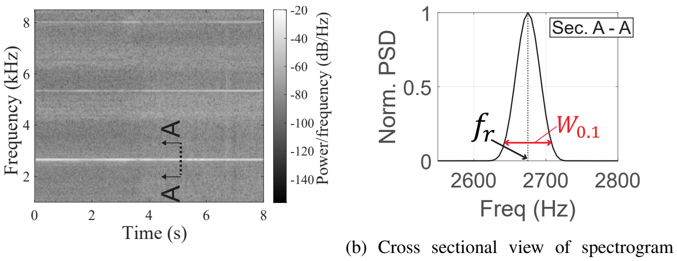

(a) Spectrogram

(b) Cross sectional view of spectrogram taken from Section A-A

Fig. 5: Spectrogram example of L=90 mm resonant tube and definition of f_r in the spectrogram.

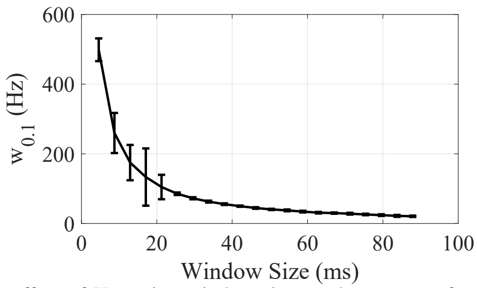

Fig. 6: The effect of Hamming window size on the resonant frequency lobe when computing spectrogram.

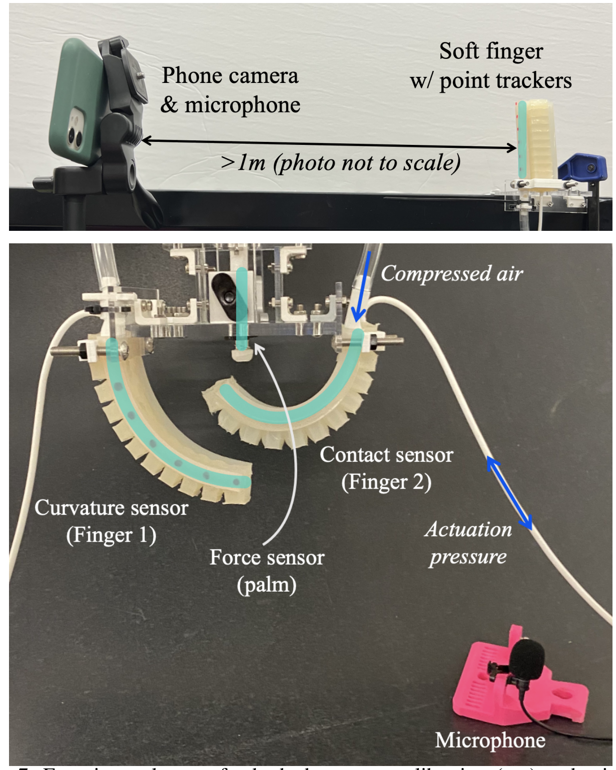

Fig. 7: Experimental setup for both the sensor calibration (top) and gripper experiments (bottom). Resonant tubes are highlighted in cyan. The microphone is either built-in to the iPhone or plugged into a GoPro camera, and the microphone is located approximately 1m from the resonators.

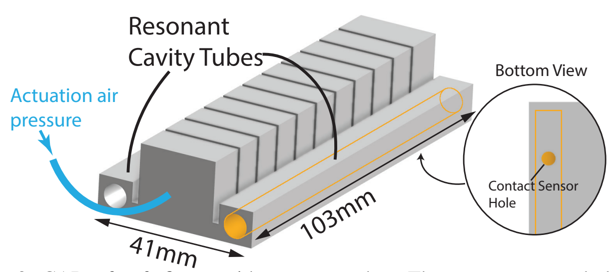

Fig. 8: CAD of soft finger with resonant tubes. The contact sensor hole is located near the distal tip of the finger on the volar side. A fipple is fitted to the resonant cavity tube opening. The finger is actuated by pressurizing the central bladder chamber.

detect as sound. The inlet is connected to a compressed air line by flexible hosing with a 8.3 mm (3/8") outer diameter, and the hose is over 4 m long with air pressure less than 34 kPa (5 psi). The resonant chambers, those described in Sections IV and V, are then attached to the other end with a press fit. One fipple is dedicated to each sensor, therefore the integrated gripper in Sec. VI utilizes multiple fipples. We use a robot arm (UR-10, Universal Robots) and 6DOF wrist force/torque sensor (Axia80, ATI) for the following experiments. The experimental setup for pose estimation and gripper demo is depicted in Fig. 7. Sound is recorded with a smartphone (iPhone 11) at a sampling rate of 44.1 kHz for experiments in Section IV and Section VI, and with an omnidirectional microphone at 48 kHz for experiments in Section V. The microphones are located approximately one meter from the resonators.

We analyze the audio recording to obtain the power spectral density (PSD) and compute resonant frequency (f_r). The spectrogram in Fig. 5a shows an example of the different resonant modes of acoustic emission from the fipple and resonant tube (90 mm in length, and 7.1 mm in diameter). We compute the f_r by choosing the frequency with the highest PSD as shown in Fig. 5b. Throughout the process, we utilized built-in functions in Matlab: $spectrogram()$ for PSD and $tfridge()$ for f_r.

In computing the spectrogram, sampling window duration affects the PSD lobe width and thus affects the separation between f_rs from different sensors. We define $W_{0.1}$ as the width of the PSD lobe at 10% of the peak PSD value. Fig. 6 shows that the small Hamming window size (< 20 ms) results in significantly wider $W_{0.1}$. Although the smaller window may update the information faster with low delay, the wide lobe allows fewer sensors not to overlap their f_r lobes. Because the $W_{0.1}$ does not decrease much for window size greater than 30 ms, we chose 33 ms as the Hamming window duration.

IV. Resonant Soft Finger

A. Implementation

We integrate the resonant pneumatic tactile sensor on a soft pneumatically-driven finger to measure proprioceptive curvature and detect contact. We use the design of soft robotic gripper in *Soft Robotics Toolkit* [16] with a modified base layer to accommodate the resonant cavity tubes, as shown in Fig. 8. We cast the array of actuating bladders first and then cast the base layer with the resonant tube after the initial array is cured. The diameter of the tube is 6 mm and the length is 10 cm. Unlike the design in [16], we do not use any inextensible intermediate layers to simplify the fabrication process, and the entire body is silicone (Dragon Skin™ 30). Two resonant tubes are on either side of the finger, maintaining symmetric free curling motion because each chamber structure stiffens its side of the finger. On a single finger, one tube can be used to measure pose while the other detects contact.

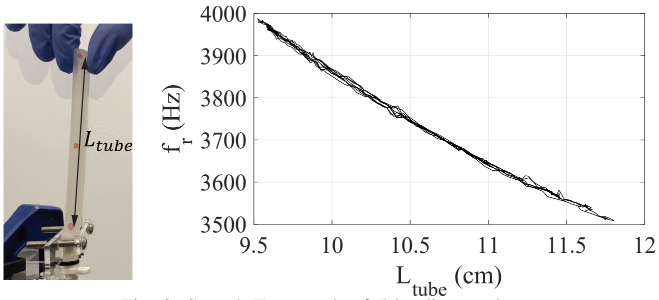

Fig. 9: Stretch Test result of 5 loading cycles.

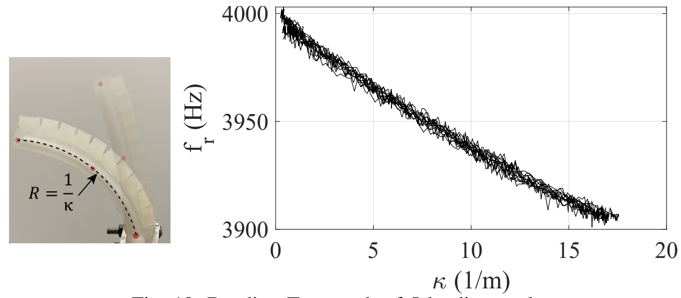

Fig. 10: Bending Test result of 5 loading cycles.

B. Pose estimation

We estimate the pose, or curvature of the gripper by measuring tube elongation. We first measure the resonant frequency (f_r) as the tube undergoes axial stretching. As shown in Fig. 9, we manually pulled a sample tube that was cutoff from the gripper in Fig. 8 left. We mark three red dots along the tube and track their location as we gently cyclically stretch the tube for 5 times. Fig. 9 right shows that f_r decreases as the tube elongates. Our sensor shows very low hysteresis unlike previous piezo-resistive bending sensors [8], [9].

Then, we test pose estimation using the pneumatic finger with the resonant tube integrated. We measure the curvature by detecting the three red dots marked on the gripper, assuming circular curvature passing through three three marker locations. The result in Fig. 10 shows similar trends in f_r: the higher the curvature, the lower the f_r, and low hysteresis.

C. Contact sensing

We also characterize how frequency changes as the lateral opening on the fingertip is occluded. To test the contact sensing performance, we made a separate tube 11 cm long, using the same material as the soft fingers. We punched a hole (D=3.2 mm) at 10 mm from the distal end as shown in Fig. 8. Then, we placed the tube on top of a flat surface and slowly lowered a flat acrylic plate over the hole using the robot arm depicted in Fig. 11 left. We decremented the gap distance (h) while measuring the wrist force/torque sensor mounted on the robot arm. At close vicinity of the hole, decrements are 0.2 mm. At each h, we measured f_r for 330 ms and report the average f_r from each h in Fig. 11 (right). The distance $h = 0$ is determined as the point where the force/torque sensor measures a large change in the contact force.

Fig. 11 shows a gradual change in f_r with values of $h < 10\,mm$. Resonant frequency plateaus for $h > 10\,mm$ while the most signal change occurs between $0 < h < 2\,mm$. When the hole is clogged ($h < 0$), f_r saturates with respect to contact force. Contact vicinity sensing is particularly useful for controlling the soft gripper [17] because the inner surface of the gripper may not conform tightly to an object surface due to the curvature or weak grasp force. Soft finger sensor performance characteristics are listed in Table I.

V. Resonant Force Probe

We present an alternative, rigid tube design characterization that uses the same principles as the soft finger, now implemented as a force probe for the gripper palm.

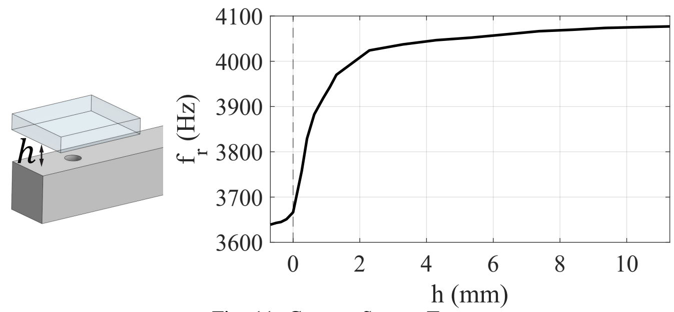

Fig. 11: Contact Sensor Test

Characteristic	Length (L_{tube})	Curv. (κ)	Contact (h)
Unloaded frequency [Hz]	3988	4003	4077
Full-scale output [Hz]	479	102	342
Dynamic range tested	2.3 cm	17.3 m^{-1}	0 - 2 mm

TABLE I: Soft sensor performance characterization from the stretch, bending and contact test.

A. Implementation

This rigid resonant tube, shown in Fig. 12, is constructed using 3D printed PLA parts and telescoping aluminum tubes. A spherical PLA end-cap plugs the tube on the opposing end of the fipple. A thin foam is placed on the end-cap inside the tube to dampen pressure waves. The telescoping aluminum tubes have a clearance fit, which results in low sliding friction and low air leakage. The outer tube has an outer diameter of 7.1 mm (9/32").

For the purpose of characterization across different tube geometries and large length displacements, we test two different tube lengths, where the fipple edge to end distance when unloaded is either 90 mm (Test Taxel 1) or 130 mm (Test Taxel 2). The maximum displacement for both taxel designs is 25 mm. A spring restores the full length of the tubing when the taxel is unloaded. We test two different spring stiffnesses: 0.19 and 1.76 N/mm. For the gripper palm probe, we created a more compact version, with the resonant tube at 10 mm long when unloaded and a restoring spring stiffness of 1.0 N/mm.

Fig. 13 shows an example audiospectrogram of Taxel 1 during 5 compression cycles. Contact force decreases tube length and increases frequency, such that lower frequency is emitted when the taxel contact is unloaded. The fundamental frequency (n=1) is seen around 3 kHz and the second harmonic (n=2) is fainter in amplitude at about 6 kHz.

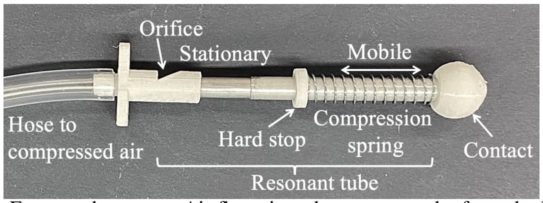

Fig. 12: Force probe sensor. Air flows into the resonant tube from the left and out from the orifice above. Telescoping rods are employed to change the tube length; one is fixed and the other moves based on the force at the contact and stiffness of the spring. A hard stop is used to keep the mobile rod from falling out of the acrylic mounting structure (not shown).

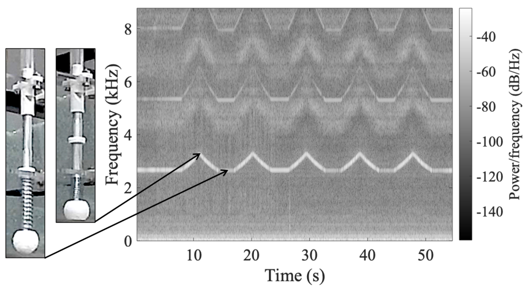

Fig. 13: Audiospectrogram of Test Taxel 1 for 5 loading cycles.

Characteristic	$\mathrm{T}_{1,\ \mathrm{soft}}$	$\mathrm{T}_{1,\ \mathrm{stiff}}$	$\mathrm{T}_{2,\ \mathrm{soft}}$
Unloaded frequency [Hz]	2650	2650	1840
Full-scale output (FSO) [Hz]	730	730	310
Dynamic range [N]	6.5	56	6.5
Sensitivity [Hz/N]	113	13	48

TABLE II: Force probe sensor performance characterization. $\mathrm{T}_{1,\ \mathrm{stiff}}$ dynamic range is linearly interpolated.

B. Force sensing

We characterize the force sensor by rigidly mounting each taxel onto the robot arm and cyclically loading it at 6.2 mm/s against a rigid surface. Audio measurements are manually synced in post-processing. Characterizations for three combinations of force probe tube length and spring stiffness are presented in Table II. The unloaded frequency of Taxel 2 ($T_{2,\ \mathrm{soft}}$) is lower than Taxel 1 ($T_{1,\ \mathrm{soft}}$) as it has a longer resonance cavity. Taxel 2 also has a lower full-scale output, expected from (1). The outputs of the two sensors with different tube lengths reside in frequency bands that do not overlap, allowing simultaneous measurements of the two. As expected, using the stiffer spring alters the sensitivity of Taxel 1 ($T_{1,\ \mathrm{stiff}}$).

The calibration curves from 10 loading cycles for displacement and force are shown in Fig. 14, comparing $T_{1,\ \mathrm{soft}}$ and $T_{1,\ \mathrm{stiff}}$. The variation in displacement from the different springs, as seen in Fig. 14, is likely due to internal flexing of the acrylic mounting structure when subject to higher forces. Taxel sensitivity is linearly fit to all data, despite hysteresis that likely resulted from friction between the telescoping aluminum tubes. As a measure of sensor noise, the unloaded, or fully extended, frequency of Taxel 1 is recorded over 20 sec and results in a standard deviation of 1.65 Hz.

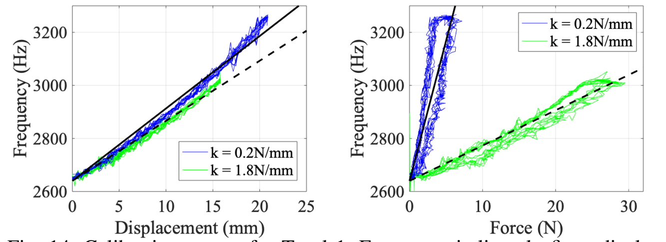

Fig. 14: Calibration curves for Taxel 1. Frequency is linearly fit to displacement (top) and force (bottom). The soft spring is shown in blue and the stiff in green. 10 cycles are plotted.

VI. ROBOTIC HAND DEMONSTRATION

We integrate two resonant soft fingers for opposed grasping on a robotic arm. We utilize the resonance tube in one finger for pose estimation and a tube in the other finger for contact sensing. Between the two fingers, the gripper palm has a resonant force probe. We demonstrate function of sensing modalities during object pick up and grasp failure of a rectangular and circular foam object, showing varied gripper states represented in these sensor signals. While these two objects happen to also be soft, this sensitive soft gripper is applicable to objects with a variety of shapes and hardness. A video of these tasks is provided in supplemental media.

A. Gripper integration

We clamp the base of the soft fingers to the rigid palm base, shown in Fig. 7. A force probe is integrated in the center or the gripper, or palm. The inner distance between the two fingers is 108 mm (4 1/4”). The fingers are offset from the center by 26 mm (1.02”) so they can curl fully without touching one another. The gripper design is not optimal and serves only as a platform to demonstrate the sensing modalities. The soft fingers are actuated by manual pressurization with 100 mL syringes. We sense curvature on Finger 1 (left) and contact on Finger 2 (right). The curvature sensor uses a different fipple geometry so the frequency ranges of the sensors are distinct for ease of processing. The gripper is mounted onto the robotic arm with wrist force/torque sensing for the following grasping tasks.

B. Grasping tasks

Resonant tactile sensing is demonstrated for the grasping of a rectangular and cylindrical shaped foam object. Prior to grasping, both objects start on the table directly below the gripper. In state (1), the object is centered between the fingers and is not in contact with the gripper. In Fig. 15 towards the end of state (1), pressure increases and we detect an increase in curvature in the left (and right) finger. The fingers bend to grasp the cylindrical object, with an asymmetric pinch achieved by pressurizing Finger 1 more than Finger 2. We detect contact on Finger 2, demarcated by a sharp decrease in resonant frequency from A to B. During state (2), the object is in a steady grasp. As the object is pulled out of grasp, we observe an increase in frequency from B to A as contact is broken. In state (3), the object is no longer in the grasp and fingers are de-pressurized to state (4). This task shows how

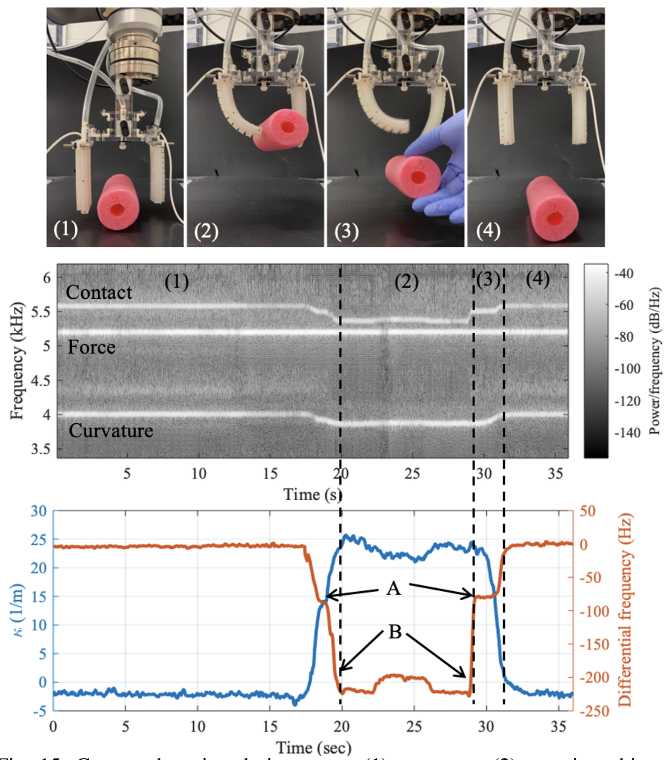

Fig. 15: Contact detection during grasp. (1) pre-grasp. (2) grasping object. (3) object is pulled out and fingers are still curled. (4) uncurling fingers. We observe a sharp decrease in frequency from when the contact sensing hole is open (A) to closed (B). We detect a loss of contact when object is pulled out around 29 sec, and uncurl fingers.

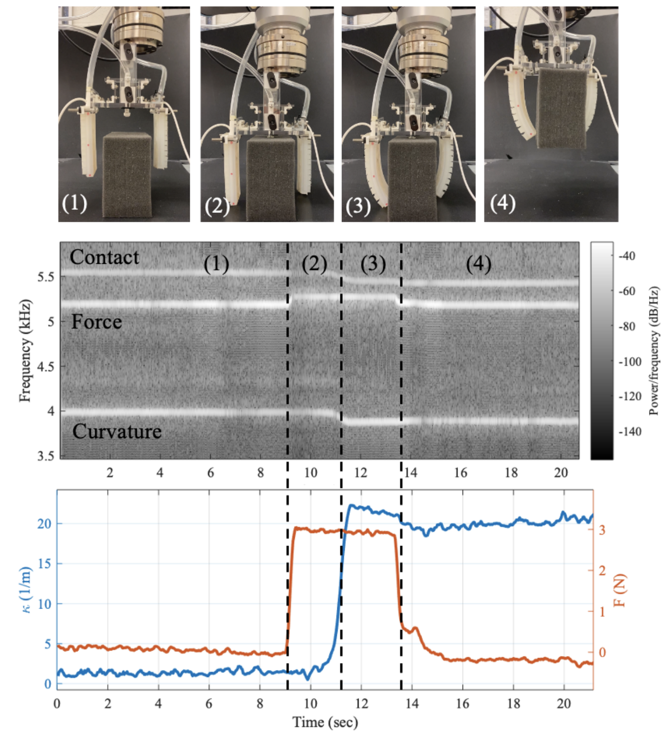

Fig. 16: Object detection in palm and grasping. (1) pre-grasp position. (2) object detected in palm by force sensor. (3) grasping of object. (4) holding lifted object. The soft fingers are holding the object up and object is no longer pushing on palm.

we can use the fingertip contact sensor to detect the presence and loss of grasped objects.

In the second task, we utilize the force sensor to detect objects in the palm to initiate grasping (Fig. 16). The robotic arm lowers the gripper until we detect palm force in state (2). The fingers close to grasp the object in state (3). The gripper lifts the object for state (4). When lifted, we do not detect force in the palm as the weight of the object pulls it away from the palm, but the constant curvature of the fingers indicate that the object remains in hand.

VII. Discussion

This resonant pneumatic tactile sensor modality opens avenues for further investigation and innovation. While we designed this sensor to emit frequencies in the human hearing range, fipples and tubes may be designed to resonate in the ultrasonic range like dog whistles [18]. These sensors would have a shorter tube length, advantageous for miniaturization. They would also not be audible or distracting to people nearby. We show three simultaneous sensing elements on the gripper. The current audio processing fails when resonant frequencies overlap. To address this, we can make resonator geometry distinct, implement pneumatic valves switching each sensor, or incorporate more robust signal processing and learning.

In addition to elongation, pinching or compressing the soft resonant tube changes its frequency. Also, by coupling contact and curvature sensing in our current design, the signals simultaneously represent both phenomenon, making it difficult to discern the two with a single resonant tube. With multiple resonant tubes in a single finger, we can use one resonant tube for pose and the other for contact. The curvature effects can then be subtracted from the contact measurements to more accurately sense contact. Alternatively, future work could include the application of machine learning methods in order to interpret these complex signals in the context of manipulation.

As previously stated, resonant frequency depends on more than geometry. No resonance is produced without air flow. Increasing flow rate in a resonant system can result in slight increases in frequency as well as sudden jumps to higher harmonics. Atmospheric conditions, such as molecular composition and temperature will affect frequency as well. Hence, the sensor is most accurate when recalibrated prior to each use, or when coupled with other sensors that can measure atmospheric conditions or flowrate.

Issues may arise if the receiver cannot monitor the emitted frequencies, potentially due to high external noises or an insulated or obstructed emitter. Note that the resonance signal was easily detectable amidst typical research laboratory noises, from anywhere in the room. In environments where external disturbances are low in amplitude or not within the sensors' frequency range, this technology provides easy-to-integrate and inexpensive sensitivity that relays a rich understanding about the forces, contacts and movements experienced by soft systems.

VIII. Conclusion

Acoustic resonance chambers can equip soft robots with pose, contact and force sensing, taking advantage of the deformation inherent to these soft structures. One major benefit of this design is that electronics can be omitted from the end-effectors of robots, while rich signals are monitored with a single remote microphone located far from contact. Thus, these sensors are simple to integrate and can operate in conditions too harsh or impractical for electrical components in the end-effector. In this study, we find that these integrated pneumatic resonant sensors provide low hysteresis and capture the state of a soft gripper.

References

[1] N. R. Sinatra, C. B. Teeple, D. M. Vogt, K. K. Parker, D. F. Gruber, and R. J. Wood, "Ultragentle manipulation of delicate structures using a soft robotic gripper," *Science Robotics*, vol. 4, no. 33, p. eaax5425, 2019.

[2] S. M. G. Vidwath, P. Rohith, R. Dikshithaa, N. Nrusimha Suraj, R. G. Chittawadigi, and M. Sambandham, "Soft robotic gripper for agricultural harvesting," in *Machines, Mechanism and Robotics*, R. Kumar, V. S. Chauhan, M. Talha, and H. Pathak, Eds. Singapore: Springer Singapore, 2022, pp. 1347–1353.

[3] R. S. Dahiya, G. Metta, M. Valle, and G. Sandini, "Tactile Sensing—From Humans to Humanoids," *IEEE Transactions on Robotics*, vol. 26, no. 1, pp. 1–20, 2010.

[4] M. T. Tolley, R. F. Shepherd, B. Mosadegh, K. C. Galloway, M. Wehner, M. Karpelson, R. J. Wood, and G. M. Whitesides, "A resilient, untethered soft robot," *Soft Robotics*, vol. 1, no. 3, pp. 213–223, 2014. [Online]. Available: https://doi.org/10.1089/soro.2014.0008

[5] F. Negrello, H. S. Stuart, and M. G. Catalano, "Hands in the real world," *Frontiers in Robotics and AI*, vol. 6, p. 147, 2020.

[6] R. L. Truby, M. Wehner, A. K. Grosskopf, D. M. Vogt, S. G. M. Uzel, R. J. Wood, and J. A. Lewis, "Soft somatosensitive actuators via embedded 3d printing," *Advanced Materials*, vol. 30, no. 15, p. 1706383, 2018. [Online]. Available: https://onlinelibrary.wiley.com/doi/abs/10.1002/adma.201706383

[7] B. Shih, C. Christianson, K. Gillespie, S. Lee, J. Mayeda, Z. Huo, and M. T. Tolley, "Design considerations for 3d printed, soft, multimaterial resistive sensors for soft robotics," *Frontiers in Robotics and AI*, vol. 6, 2019. [Online]. Available: https://www.frontiersin.org/article/10.3389/frobt.2019.00030

[8] T. Giffney, M. Xie, A. Yong, A. Wong, P. Mousset, A. McDaid, and K. Aw, "Soft pneumatic bending actuator with integrated carbon nanotube displacement sensor," *Robotics*, vol. 5, no. 1, pp. 1–9, 2016.

[9] A. Koivikko, E. S. Raei, M. Mosallaei, M. Mäntysalo, and V. Sariola, "Screen-printed curvature sensors for soft robots," *IEEE Sensors Journal*, vol. 18, no. 1, pp. 223–230, 2018.

[10] W. E. Heap, N. D. Naclerio, M. M. Coad, S.-G. Jeong, and E. W. Hawkes, "Soft retraction device and internal camera mount for everting vine robots," in *2021 IEEE/RSJ International Conference on Intelligent Robots and Systems (IROS)*, 2021, pp. 4982–4988.

[11] G. Zöller, V. Wall, and O. Brock, "Acoustic sensing for soft pneumatic actuators," in *2018 IEEE/RSJ International Conference on Intelligent Robots and Systems (IROS)*, 2018, pp. 6986–6991.

[12] S. T. Mahon, A. Buchoux, M. E. Sayed, L. Teng, and A. A. Stokes, "Soft robots for extreme environments: Removing electronic control," in *2019 2nd IEEE International Conference on Soft Robotics (RoboSoft)*, 2019, pp. 782–787.

[13] D. Drotman, S. Jadhav, D. Sharp, C. Chan, and M. T. Tolley, "Electronics-free pneumatic circuits for controlling soft-legged robots," *Science Robotics*, vol. 6, no. 51, p. eaay2627, 2021. [Online]. Available: https://www.science.org/doi/abs/10.1126/scirobotics.aay2627

[14] K. Higashi, S. Okamoto, and Y. Yamada, "What is the Hardness Perceived by Tapping?" in *Haptics: Perception, Devices, Control, and Applications*, ser. Lecture Notes in Computer Science, F. Bello, H. Kajimoto, and Y. Visell, Eds. Cham: Springer International Publishing, 2016, pp. 3–12.

[15] J. W. Coltman, "Sounding mechanism of the flute and organ pipe," *The Journal of the Acoustical Society of America*, vol. 44, no. 4, pp. 983–992, 1968. [Online]. Available: https://doi.org/10.1121/1.1911240

[16] D. P. Holland, E. J. Park, P. Polygerinos, G. J. Bennett, and C. J. Walsh, "The soft robotics toolkit: Shared resources for research and design," *Soft Robotics*, vol. 1, no. 3, pp. 224–230, 2014.

[17] Y. Li, Y. Chen, and Y. Li, "Pre-charged pneumatic soft gripper with closed-loop control," *IEEE Robotics and Automation Letters*, vol. 4, no. 2, pp. 1402–1408, 2019.

[18] S. M. Topman and M. C. Sharp, "Whistle," Mar. 2 2004, US Patent 6,698,377.